

# Thermally Controllable High-Efficiency Unidirectional Coupling in a Double-Slit Structure Filled With Phase Change Material

Volume 11, Number 2, April 2019

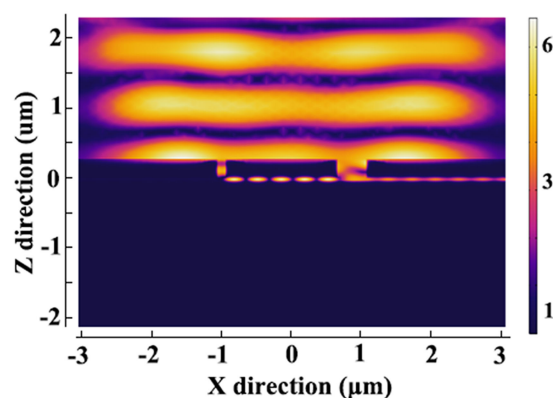
Mehdi Afshari-Bavil

Mingli Dong

Chuanbo Li

Shuai Feng

Lianqing Zhu



---

DOI: 10.1109/JPHOT.2019.2907611

1943-0655 © 2019 IEEE

# Thermally Controllable High-Efficiency Unidirectional Coupling in a Double-Slit Structure Filled With Phase Change Material

Mehdi Afshari-Bavil<sup>1,2</sup>, Mingli Dong,<sup>1,2</sup> Chuanbo Li<sup>1,3</sup>,  
Shuai Feng<sup>1,3</sup> and Lianqing Zhu<sup>1,2</sup>

<sup>1</sup>Joint International Research Laboratory of Advanced Photonics and Electronics, Beijing Information Science and Technology University, Beijing 100192, China

<sup>2</sup>Beijing Key Laboratory for Optoelectronic Measurement Technology, Beijing Information Science and Technology University, Beijing 100192, China

<sup>3</sup>School of Science, Minzu University of China, Beijing 100081, China

DOI:10.1109/JPHOT.2019.2907611

1943-0655 © 2019 IEEE. Translations and content mining are permitted for academic research only.  
Personal use is also permitted, but republication/redistribution requires IEEE permission.  
See [http://www.ieee.org/publications\\_standards/publications/rights/index.html](http://www.ieee.org/publications_standards/publications/rights/index.html) for more information.

Manuscript received February 27, 2019; revised March 22, 2019; accepted March 23, 2019. Date of publication March 26, 2018; date of current version April 11, 2019. This work was supported by the program for Changjiang scholars and innovative research team in university under Grant IRT-16R07. Corresponding authors: Mehdi Afshari-Bavil and Chuanbo Li (e-mail: mehdi.afshari@bistu.edu.cn; cbli@muc.edu.cn).

**Abstract:** We present the realization of a high-efficiency, compact, and thermally tunable unidirectional launcher of surface plasmon polaritons (SPPs) in a double-slit structure filled with phase change materials (PCMs). PCMs such as VO<sub>2</sub> provide a feasible way for tailoring optical properties, particularly refractive index as a function of heat. By introducing a narrow hybrid dielectric layer beneath the slits, SPPs couple efficiently into waveguide mode and propagate within the slot waveguide with considerably high intensity. Our simulation results revealed up to 80% coupling efficiency into the slot waveguide with extinction ratio of 1:800 between the left and the right slots can be achieved at telecommunication wavelength for normally incident P-polarized light. By heating the coupler above the VO<sub>2</sub> phase transition temperature, the coupling and consequently the crosstalk approaches zero. Propagation length and other properties of the structure are characterized to confirm the feasibility of the coupler. This approach of unidirectional coupling into slot waveguides may lead to the development of integrated plasmonic circuits and on-chip applications.

**Index Terms:** Plasmonics, subwavelength structures.

## 1. Introduction

The rigid tendency for the miniaturization of communication systems has compelled researchers to design optical integrated circuits beyond the diffraction limit. This target can be achieved by exploiting surface plasmon polaritons (SPPs), which are propagating transverse magnetic waves at the interface of a dielectric–metallic layer [1], [2]. To fully develop plasmonic chips, various phenomena associated with excitation, propagation, and scattering of SPPs should carefully be addressed [3]–[6]. Considering mismatch in light and SPPs wave vectors, normal illumination cannot excite SPPs, unless gratings, slits, holes, or any symmetry broken configurations are implemented [7], [8]. The most successful SPPs generator is Bragg grating, which is composed of some periodic

grooves that can excite SPPs and directionally guide them toward the desired direction [9]. Two main figure-of-merits for SPPs launchers are the coupling efficiency and extinction ratio, which demonstrates the ratio between intensity along the desired direction and the opposite direction. The tradeoff between the coupling efficiency, the extinction ratio and footprint always was an indispensable task. Single hole or slit, hole or slit with corrugated grooves, metasurfaces and double slits with equal and unequal widths have been offered as unidirectional propagation features with acceptable coupling efficiency, extinction ratios, and small footprint [10]–[14]. Alternatively, for plasmonic on-chip applications, the active control of light propagation and unidirectional propagation by external stimuli has attracted recent research attention. Numerous electrically and all optically controlled schemes by exploiting the electro-optical effect have been proposed, characterized, and fabricated [15]–[17]. Previously, we introduced an active unidirectional launcher based on a double-slit structure that yields directional propagation at the desired direction with 55% coupling efficiency and extinction ratio of 1:70 under external voltage [18]. However, the fabrication process for electro-optical materials remains a major challenge.

Phase change materials (PCMs), such as vanadium dioxide ( $\text{VO}_2$ ) [15], [19]–[22] and GeSbTe [23]–[25] have superior characteristics to actively control light in the telecommunication regime because of their phase transition from insulator to metal. However our particular attention is  $\text{VO}_2$  to assure the proof-of-concept feasibility due to similarity with the fabricated configuration that has been reported by Kocer *et al.* [26]. At the transition temperature of 68 °C,  $\text{VO}_2$  undergoes a reversible phase change on picosecond timescale. As the temperature increases Metallic Island inside the insulator  $\text{VO}_2$  is created and at transition temperature entire the  $\text{VO}_2$  film eventually becomes metallic. This transition can be triggered by different stimuli, such as strain, current, voltage, and optical pumping, but most typically by increasing temperature. The mechanism for this transition completely has been calculated from basic principles using Peierls instability coupled with an enharmonic phonon contribution [27]. The transition is accompanied with a large variation in refractive index. In the telecommunication regime at a wavelength of 1550 nm, the refractive index in insulating phase is about  $3 + 0.4i$  and becomes  $2 + 3i$  in the metallic phase [28]. The effective dielectric function of  $\text{VO}_2$  film in the phase transition process can be described by Bruggeman effective medium theories [29]. Recently, a thermally tunable plasmonic absorber consisting of metallic grating with narrow slits filled by  $\text{VO}_2$  has been proposed and experimentally demonstrated [26].

We adopted the concept of metallic grating filled with  $\text{VO}_2$  with our previously reported double-slit structure and proposed a unidirectional launcher. Two unequal slits filled with  $\text{VO}_2$  is considered. To achieve the waveguide coupling mode, a narrow dielectric layer is embedded and followed by another metallic layer to sandwich the dielectric layer and make a hybrid scheme. Through analytical calculations for geometrical parameters, constructive interference occurs beneath the slits along one direction and enhances the light intensity. Numerical results based on finite element method (FEM) technique demonstrate that the proposed device offers extra-coupling efficiency up to 80% and extinction ratio of 1:800. Other features of this coupler are polarization and incidence angle dependent, single-wavelength functionality, and small footprint.

## 2. Structure Description and Theoretical Approach

A schematic of the plasmonic directional launcher with two unequal slits ( $w_1, w_2$ ) with interspace distance  $d$  milled on silver film with thickness  $t$  filled with  $\text{VO}_2$  is shown in Fig. 1. To limit SPPs propagation into a confined space, a narrow silica layer under the slits followed with one more metallic layer is introduced to make a hybrid metallic–dielectric–metallic waveguide slot. The working wavelength is in the telecommunication regime (1555 nm); light is p-polarized and impinges from the top. Line A is at the center of interspace distance, and line B is at the center of the dielectric layer; these lines are the monitoring lines for observing light intensity variations.  $d, t, w_1, w_2$ , and  $h$  are 1616, 280, 100, 400, and 25 nm, respectively. The reason why these values are chosen will be explained in the next part. The refractive index of silica is 1.36, and the refractive index data of  $\text{VO}_2$  is adopted from experimental work reported by Joushaghani *et al* [28]. For our sample at

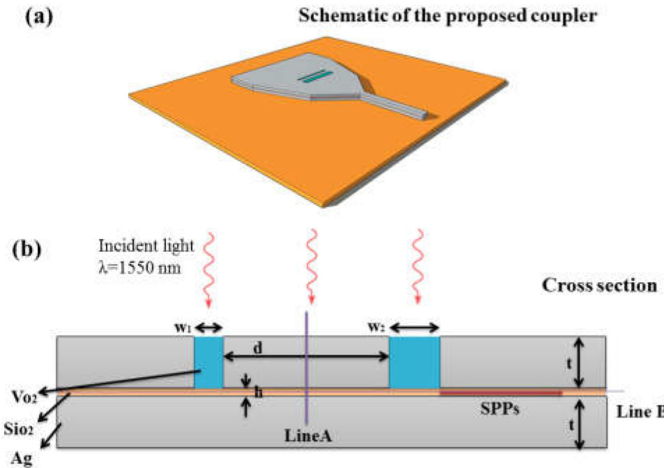


Fig. 1. (a) Schematic of the proposed structure. (b) Cross section of the structure.  $d$ ,  $t$ ,  $h$ ,  $w_1$  and  $w_2$  stands for interspace distance between slits, metallic film thickness, dielectric layer thickness and slits width, respectively. Line A and B are monitoring lines. The incident light is P-polarized and impinges from top.

1555 nm, the refractive index for the insulating phase is about  $3 + 0.4i$ , and permittivity of silver is represented by Drude model:

$$\varepsilon = \varepsilon_\infty - \frac{\omega_p^2}{\omega^2 + i\omega\Gamma} \quad (1)$$

where high-frequency bulk permittivity  $\varepsilon_\infty = 4.2$ , bulk plasmon frequency  $\omega_p = 1.346 \times 10^{16}$  rad/s, and electron collision frequency  $\Gamma = 9.617 \times 10^{13}$  rad/s [30]. SPPs can only be excited by p-polarized light so the structure has inherently polarization dependence feature. For a profound analysis of structure, we have performed numerical calculation based on two dimensional FEM technique. The structure can be fabricated by using magnetron sputtering to deposit a silver layer and silica. Subsequently, focused ion beam milling of the slits can be perforated. Finally, VO<sub>2</sub> can be filled inside the slits by using conventional e-beam lithography and deposition techniques.

Subwavelength slits in a metallic film can excite SPPs by compensating the necessary momentum for the SPPs excitation modes. A portion of incident radiation propagates through the slits and partially scatters into free-space radiation at the exit aperture. The remainder propagates on the metal–dielectric interface. The hybrid configuration leads all the light at the exit aperture to propagate inside the narrow slot. A raw approximation about the thickness of the hybrid layer is that it should be about the penetration depth of SPPs, which for silver is about 27 nm [1].

The slits can be considered as Fabry–Perot (FP) resonator with two open ends. Due to multi-reflection effect inside the slit an effective refractive index ( $N_{eff}$ ) that is larger than the air refractive index and strongly depends on the slit width, incident wavelength, and dielectric medium can be introduced. In reference [31] an analytical relationship for  $N_{eff}$  has been introduced that the slit width inversely affects  $N_{eff}$ . Therefore narrow slits yield in large effective refractive indexes. The values of  $N_{eff}$  for our desired parameters are obtained from our previously reported result [18]. Therefore, by changing the slit width or dielectric medium inside the slits, different phase retardation can be imposed on travelling SPPs through the slit. The present study aims to obtain the geometrical parameters that cause SPPs constructively interfere along one direction on the unilluminated surface while destructively along the opposite direction [11]. To attain this goal, the relative phases of SPPs at two exit apertures should be correlated with each other through a proper interspace

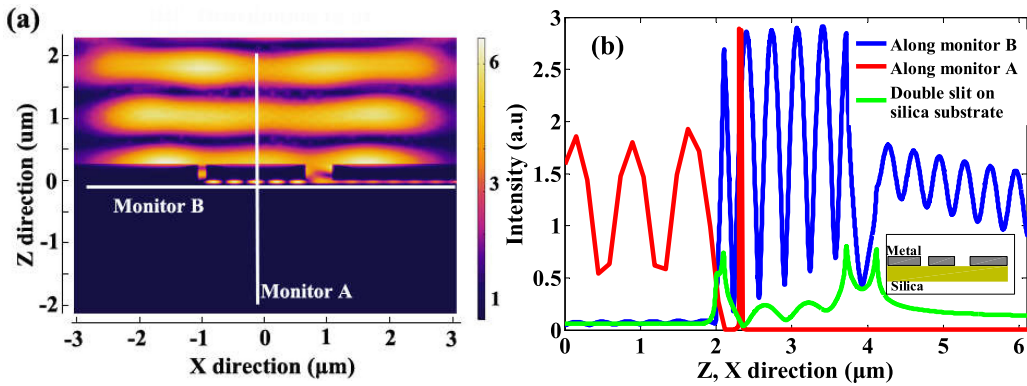


Fig. 2. (a) Magnetic field distribution of our proposed unidirectional launcher; (b) axial field intensity along monitor A (red line) and B (blue line). Green line is the intensity profile of double slit structure when the lower metallic layer is replaced by silica. The inset shows a double slit structure on silica substrate.

distance [11]:

$$\phi_1 + d \frac{2\pi}{\lambda_{SP}} = \phi_2 + 2M\pi \quad (2)$$

$$\phi_2 + d \frac{2\pi}{\lambda_{SP}} = \phi_1 + (2M + 1)\pi \quad (3)$$

where  $\phi_1$  and  $\phi_2$  are the relative phases of travelling SPPs at the exit apertures for the left and right slits, respectively;  $\lambda_{SP}$  is the SPPs wavelength given by  $\lambda_{SP} = \lambda(\frac{\varepsilon + \varepsilon_d}{\varepsilon \varepsilon_d})^{1/2}$ ;  $\varepsilon$  and  $\varepsilon_d$  are the dielectric functions of metal and dielectric medium, respectively;  $d$  is the interspace distance; and  $M$  is an arbitrary integer. The relative phase of each slit can be obtained by  $\phi_{1,2} = N_{eff1,2}2\pi t/\lambda$ , where  $t$  is the film thickness,  $\lambda$  is the wavelength of incident light, and  $N_{eff1,2}$  are the effective refractive index of the left and right slits with slit width  $w_1$  and  $w_2$ , respectively. If  $t$  is a given value, then the equation can be solved for  $d$  when  $M = 1$ :

$$d = \left( \frac{\Delta N_{eff}}{\lambda} + 1 \right) \lambda_{SP} \quad (4)$$

where  $\Delta N_{eff}$  is the difference of effective refractive indexes of the slits.

### 3. Result and Discussion

For our considered slits, the effective refractive indexes at the mentioned wavelengths are 1.208 and 1.055, respectively. For  $t = 280$  nm and our working wavelength;  $d$  is obtained from Eq. (4) to be 1616 nm. Other values of  $M$  can yield high orders of interspaces. At this distance, maximum unidirectional propagation is observed. However, high orders should have low intensity due to the propagation loss that occurs for travelling SPPs along the surface. Fig. 2(a) shows the magnetic field distribution. The slot thickness numerically is swept to optimize the result; the optimized value for slot thickness is determined to be 25 nm. The magnetic field at the undesired direction because of destructive interferences is completely quenched. Fig. 2(b) depicts the light intensity along monitors A (red line) and B (blue line) when  $VO_2$  is in dielectric phase. The green line is the intensity of double slit structure along monitor B where the lower metallic layer is replaced by silica as demonstrated in the inset of Fig. 2(b).

Some results can be extracted from this figure. 1) The hybrid structure amplifies unidirectional light intensity by approximately 50-fold. 2) The coupling efficiency is more than 80%, which is considerably high. The average light intensity inside the hybrid layer at short distances does not have considerable variation with the average intensity on top of the metallic surface. 3) The obtained

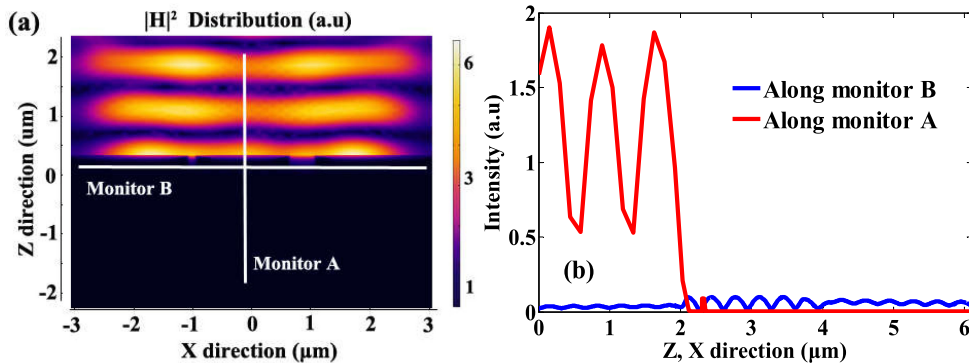


Fig. 3. (a) Magnetic field distribution of our proposed directional launcher when  $\text{VO}_2$  is in metallic phase. (b) Axial field intensity along monitor A (red line) and B (blue line). In metallic phase no lights enter to the slot waveguide. The result is valid for entire wavelength range.

extinction ratio  $E_L:E_R$  is 1:800, which is impressively large compared with reported results. 4) The periodic behavior of the light inside the slots is equal to SPPs wavelength inside the slot. 5) The propagation length or distance where intensity of SPPs drops to  $1/e$  of its maximum value is  $8.5 \mu\text{m}$ .

Similar results can be obtained in passive unidirectional launchers. To reveal the role of  $\text{VO}_2$ , we allow  $\text{VO}_2$  to undergo transition from insulator to metallic phase. This transition can be initiated by different stimuli, such as heating, optical pumping, voltage, or current. A feasible technique to heat the  $\text{VO}_2$  without major effect on the overall response of the whole configuration is heating electrically by separated electrodes for each slit [32], [33]. Thermal expansion of substrates that widely has been investigated by different groups is an effect that can affect  $\text{VO}_2$  films, especially thick films through their plasma frequency [34]. However in our case because  $\text{VO}_2$  film is not thick and has small volume; so this effect was neglected [28]. Moreover when the structure is heated, it is expected the system hinder the light propagation so any unwanted thermal expansion assists in the structure functionality.

Once the sample is heated above the transition temperature ( $68^\circ\text{C}$ ), the refractive index is altered and becomes about  $2 + 3i$  at our working wavelength. Fig. 3(a) shows the field distribution when  $\text{VO}_2$  is in the metallic phase. The amount of light enters to the slot waveguide is negligible. As shown in Fig. 3(b), the axial field intensity along monitor B verifies that no SPPs propagate inside the slot. The phase change transition is reversible on the picosecond time scale so we can easily switch light propagation to the slot waveguide by tuning the heat [35].

The main advantage of using PCM is minimizing crosstalk when the structure is illuminated by non-resonance wavelengths. However, in the structure designed to deliver unidirectional coupling at the desired wavelength, a large portion of light as crosstalk can travel through the slits and equally propagate toward left and right waveguides. When  $\text{VO}_2$  undergoes transition and transforms into a metal, the imaginary part of refractive index increases sharply and causes zero transmission for the entire wavelength range.

Fig. 4(a) shows the coupling and extinction ratio as a function of wavelength for both metallic (blue) and insulating phase (red). Despite a sharp peak for the extinction ratio in insulating phase at resonance wavelength (full width at half maximum is about 10 nm), the coupling efficiency that is shown in the inset of Fig. 4(a) is about 50%. However, it is equally split in both left and right slots, so the extinction ratio is low. In the metallic phase, both coupling and extinction ratio are almost negligible. As a result for any wavelength, the crosstalk approaches zero that is critical for optical communication systems.

During the phase transition of  $\text{VO}_2$ , a structural change from a monoclinic to a tetragonal lattice structure occurs [36]. The exact mechanism has been investigated, and different mechanisms have been introduced.  $\text{VO}_2$  consists of many domains, and transition occurs gradually when different

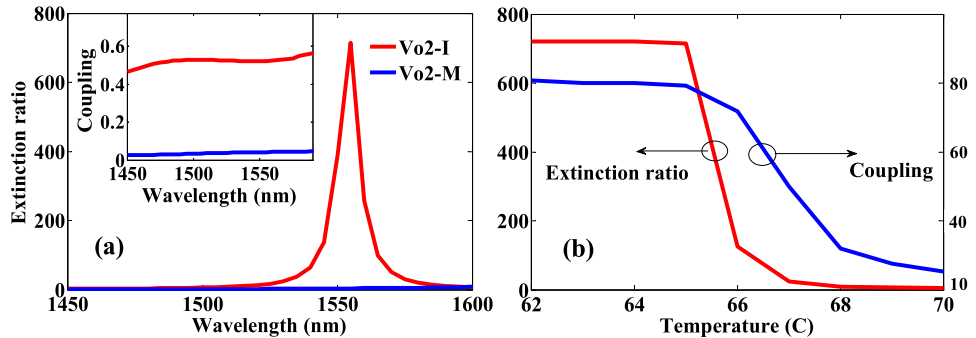


Fig. 4. (a) the extinction ratio and coupling (the inset) as function of wavelength for metallic (blue line) and insulating (red line) phase. The full width at half maximum is only 10 nm (b) Temperature dependence of coupling (blue line) and extinction ratio (red line). Both parameters drop abruptly when the transition happen at temperature 68 °C.

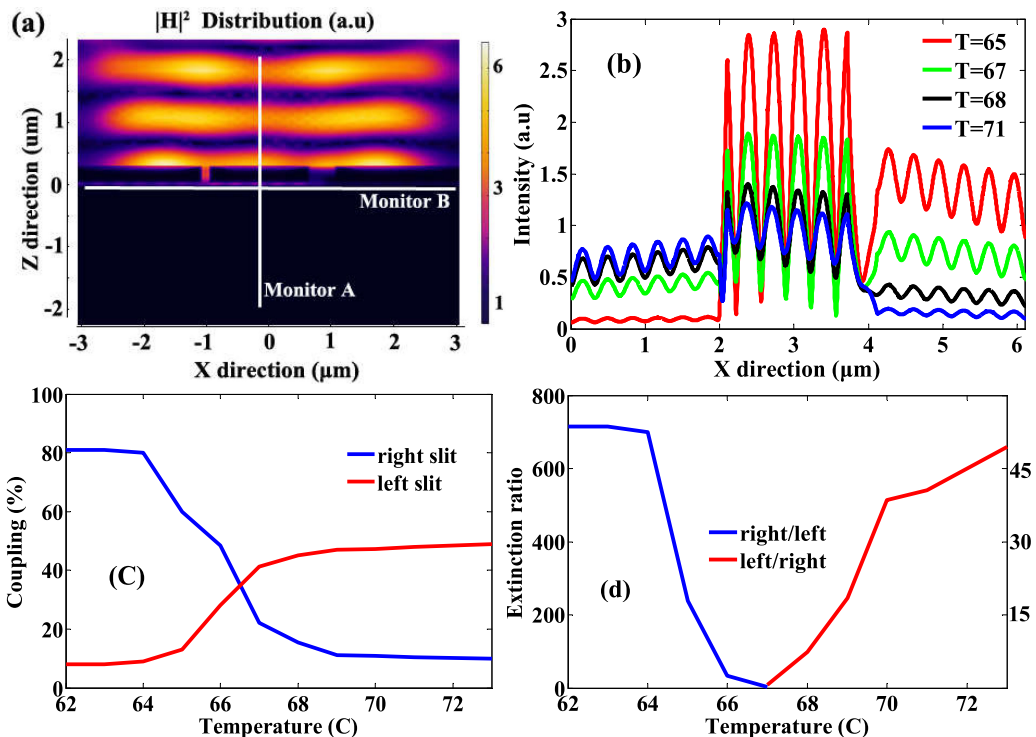


Fig. 5. (a) Magnetic field distribution when left slit is in insulator phase and right slit in metallic phase; (b) axial field intensity along monitor B for different temperatures. (c) Coupling and (d) extinction ratio as function of temperature.

domains undergo transition at different temperatures. Thus, the refractive index changes gradually. By increasing heat, the metallic portion of VO<sub>2</sub> increases and becomes fully metallic above 68 °C. The temperature-dependent refractive index at telecommunication wavelength is extracted from reference [37]. Consequently, the coupling and extinction ratio versus temperature is shown in Fig. 4(b). Both parameters abruptly drop when the temperature is above the transition temperature. Intermediate values for the coupling and extinction ratio can be realized as a tunable intensity coupler.

If the left slit is kept in insulator phase and the right slit undergoes transition, then a switchable unidirectional transition can be achieved. The proof-of-concept can be accomplished by replacing

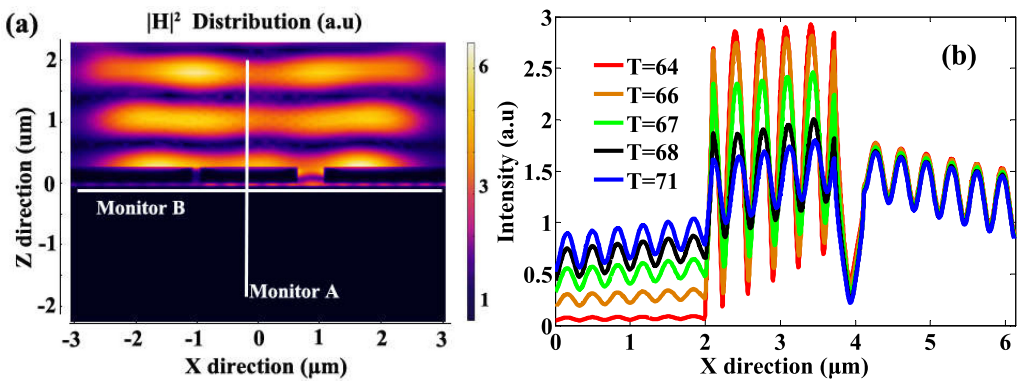


Fig. 6. (a) Magnetic field distribution when right slit is in insulator phase and left slit is in metallic phase; (b) axial field intensity along monitor B for different temperatures.

$\text{VO}_2$  in the left slit with a dielectric material that has similar refractive index. Fig. 5(a) shows the magnetic field distribution when the right still is in the metallic phase while the left slit is in the insulator phase. Unidirectional coupling to the left slit can be seen. The axial field distribution along monitor B for different temperatures is presented in Fig. 5(b). By increasing temperature, light coupling can be switched from right to left. Fig. 5(c) shows the coupling of light to the left and right slots as a function of temperature. Coupling to the left slit is smaller than that to the right slot, which can be attributed to a wider slit and consequently more light flow. The maximum realized coupling efficiency is 50%. Fig. 5(d) shows the extinction ratio as a function of temperature. The left axes are the extinction ratio upon coupling into the right slot (blue line), whereas the right axes are the extinction ratio when coupling into the left slot (red line) occurs. The maximum obtained extinction ratio is 22:1, which is much smaller than the corresponding ratio to the right slot.

Finally, we considered phase transition for left slit, whereas the right slit is in the insulator phase. By increasing temperature, the portion of light begins to move toward the left slot. Maximum coupling of 55% is realized when the left slit is fully in the metallic phase. However, coupling to the right slot does not change considerably. The extinction ratio also drops sharply and approaches 1:2.6. Fig. 6(a) shows the magnetic field distribution when the left slit is fully metallic and the temperature is higher than the transition temperature. Fig. 6(b) shows the axial field distribution along monitor B for different temperatures.

#### 4. Conclusion

For the first time, by utilizing PCM in a double-slit structure, we theoretically proposed and investigated a SPPs unidirectional launcher and coupler in the same structure for telecommunication wavelength with super high extinction ratio of 1:800, coupling efficiency of more than 80%, and small footprint. The structure is polarization and incident angle dependent and has no crosstalk for non-resonance wavelengths when  $\text{VO}_2$  undergoes phase transition. Moreover, the structure is designed to respond at a single wavelength. For any desired wavelength, proper geometrical parameters can be determined accordingly. Our results may have potential applications in plasmonic integrated circuits and on-chip applications.

#### References

- [1] S. A. Maier, *Plasmonics: Fundamentals and Applications*. Berlin, Germany: Springer, 2007.
- [2] A. V. Zayats and S. A. Maier, *Active Plasmonics and Tunable Plasmonic*. Hoboken, NJ, USA: Wiley, 2013.
- [3] M. A. A. Bavil, L. Gao, and X. Sun, "A compact nanoplasmonics filter and intersection structure based on utilizing a slot cavity and a Fabry-Perot resonator," *Plasmonics*, vol. 8, pp. 631–636, 2013.

- [4] M. A. Baval, Z. Liu, W. Wu, and C. Li, "Photocurrent enhancement in Si-Ge photodetectors by utilizing surface plasmons," *Plasmonics*, vol. 12, pp. 1709–1715, 2016.
- [5] X. Wang, Z. Cheng, K. Xu, H. K. Tsang, and J.-B. Xu, "High-responsivity graphene/silicon-heterostructure waveguide photodetectors," *Nature Photon.*, vol. 7, pp. 888–891, 2013.
- [6] Y. Tsur, I. Epstein, R. Remez, and A. Arie, "Wavefront shaping of plasmonic beams by selective coupling," *ACS Photon.*, vol. 4, pp. 1339–1343, 2017.
- [7] U. Schröter and D. Heitmann, "Surface-plasmon-enhanced transmission through metallic gratings," *Phys. Rev. B*, vol. 58, 1998, Art. no. 15419.
- [8] E. Popov, M. Neviere, S. Enoch, and R. Reinisch, "Theory of light transmission through subwavelength periodic hole arrays," *Phys. Rev. B*, vol. 62, 2000, Art. no. 16100.
- [9] J. G. Rivas, M. Kuttge, P. H. Bolivar, H. Kurz, and J. A. Sánchez-Gil, "Propagation of surface plasmon polaritons on semiconductor gratings," *Phys. Rev. Lett.*, vol. 93, 2004, Art. no. 256804.
- [10] F.-F. Ren, K.-W. Ang, J. Ye, M. Yu, G.-Q. Lo, and D.-L. Kwong, "Split bull's eye shaped aluminum antenna for plasmon-enhanced nanometer scale germanium photodetector," *Nano Lett.*, vol. 11, pp. 1289–1293, 2011.
- [11] T. Xu, Y. Zhao, D. Gan, C. Wang, C. Du, and X. Luo, "Directional excitation of surface plasmons with subwavelength slits," *Appl. Phys. Lett.*, vol. 92, 2008, Art. no. 101501.
- [12] X. Li, Q. Tan, B. Bai, and G. Jin, "Experimental demonstration of tunable directional excitation of surface plasmon polaritons with a subwavelength metallic double slit," *Appl. Phys. Lett.*, vol. 98, pp. 25–27, 2011.
- [13] S. Huang, C. Y. Wang, H. Y. Chen, M. H. Lin, Y. J. Lu, and S. Gwo, "Dual-band planar plasmonic unidirectional launching in a semiannular apertures array," *ACS Photon.*, vol. 3, pp. 584–589, 2016.
- [14] F. Ding, R. Deshpande, and S. I. Bozhevolnyi, "Bifunctional gap-plasmon metasurfaces for visible light: Polarization-controlled unidirectional surface plasmon excitation and beam steering at normal incidence," *Light Sci. Appl.*, vol. 7, 2018, Art. no. 17178.
- [15] M. Rudé, R. E. Simpson, R. Quidant, V. Pruneri, and J. Renger, "Active control of surface plasmon waveguides with a phase change material," *ACS Photon.*, vol. 2, pp. 669–674, 2015.
- [16] Z. Dong *et al.*, "Electrically-excited surface plasmon polaritons with directionality control," *ACS Photon.*, vol. 2, pp. 385–391, 2015.
- [17] S. G. Rodrigo, "All-optical control of surface plasmons by second-harmonic generation," *Phys. Rev. B*, vol. 98, 2018, Art. no. 041407.
- [18] M. A. Baval, Z. Zhou, and Q. Deng, "Active unidirectional propagation of surface plasmons at subwavelength slits," *Opt. Exp.*, vol. 21, 2013, Art. no. 170676.
- [19] J. Jeong, A. Joushaghani, S. Paradis, D. Alain, and J. K. S. Poon, "Electrically controllable extraordinary optical transmission in metallic surface gratings on VO<sub>2</sub>," *Opt. Lett.*, vol. 40, pp. 4–5, 2015.
- [20] G. Kaplan, K. Aydin, and J. Scheuer, "Dynamically controlled plasmonic nano-antenna phased array utilizing vanadium dioxide [Invited]," *Opt. Mater. Exp.*, vol. 5, pp. 2513–2524, 2015.
- [21] S. J. Kim *et al.*, "Active directional switching of surface plasmon polaritons using a phase transition material," *Sci. Rep.*, vol. 7, pp. 1–8, 2017.
- [22] G. I. S. Eo *et al.*, "Facile photothermal synthesis of localized vanadium oxide capable of extraordinary phase transition," *Opt. Mater. Exp.*, vol. 7, pp. 2860–2870, 2017.
- [23] S. Abdollahramezani, H. Taghinejad, T. Fan, Y. Kiarashinejad, A. Ali, and A. Adibi, "Reconfigurable multifunctional metasurfaces employing hybrid phase-change plasmonic architecture," 2018. [Online]. Available: arXiv:1809.08907.
- [24] C. Ríos *et al.*, "Integrated all-photonic non-volatile multi-level memory," *Nature Photon.*, vol. 9, pp. 1–9, 2015.
- [25] C. Ríos, P. Hosseini, C. D. Wright, and H. Bhaskaran, "On-chip photonic memory elements employing phase-change materials," *Adv. Mater.*, vol. 26, pp. 1372–1377, 2014.
- [26] H. Kocer *et al.*, "Thermal tuning of infrared resonant absorbers based on hybrid gold-VO<sub>2</sub>nanostructures," *Appl. Phys. Lett.*, vol. 106, 2015, Art. no. 161104.
- [27] J. D. Budai *et al.*, "Metallization of vanadium dioxide driven by large phonon entropy," *Nature*, vol. 515, pp. 535–539, 2014.
- [28] A. Joushaghani, "Micro- and nano-scale optoelectronic devices using vanadium dioxide," Thesis, Department of Electrical and Computer Engineering University of Toronto, Canada, 2014.
- [29] P. U. Jepsen *et al.*, "Metal-insulator phase transition in a VO<sub>2</sub> thin film observed with terahertz spectroscopy," *Phys. Rev. B-Condens. Matter Mater. Phys.*, vol. 74, 2006, Art. no. 205103.
- [30] K. L. Shuford, M. A. Ratner, S. K. Gray, and G. C. Schatz, "Finite-difference time-domain studies of light transmission through nanohole structures," *Appl. Phys. B*, vol. 84, pp. 11–18, 2006.
- [31] S. Bozhevolnyi, *Plasmonic Nanoguide and Circuits*. Redwood City, CA, USA: Pan Stanford Publishing, 2008, pp. 10–20.
- [32] F. Xiong, A. D. Liao, D. Estrada, and E. Pop, "Low-power switching of phase-change materials with carbon nanotube electrodes," *Science*, vol. 332, pp. 568–750, 2011.
- [33] N. Yamada, *Phase Change Materials: Science and Applications*. New York, NY, USA: Springer-Verlag, 2009.
- [34] J. Sakai, M. Zaghloul, M. Matsushima, H. Funakubo, K. Okimura, and T. Raman, "Impact of thermal expansion of substrates on phase transition temperature of VO<sub>2</sub> films," *J. Appl. Phys.*, vol. 116, 2014, Art. no. 123510.
- [35] A. Cavalleri *et al.*, "Femtosecond structural dynamics in VO<sub>2</sub> during an ultrafast solid-solid phase transition," *Phys. Rev. Lett.*, vol. 87, 2001, Art. no. 237401.
- [36] A. Zylbersztejn and N. F. Mott, "Metal-insulator transition in vanadium dioxide," *Phys. Rev. B*, vol. 11, 1975, Art. no. 4383.
- [37] P. Cormier, T. V. Son, J. Thibodeau, A. Doucet, V. Van Truong, and A. Haché, "Vanadium dioxide as a material to control light polarization in the visible and near infrared," *Opt. Commun.*, vol. 382, pp. 80–85, 2017.